

# Reentrant behavior of breathing mode in one-dimensional Bose gas

A. Iu. Gudyma,<sup>1,2</sup> G. E. Astrakharchik,<sup>3</sup> and Mikhail B. Zvonarev<sup>1,2</sup>

<sup>1</sup>*Univ Paris-Sud, Laboratoire LPTMS, UMR8626, Orsay, F-91405, France*

<sup>2</sup>*CNRS, Orsay, F-91405, France*

<sup>3</sup>*Departament de Física i Enginyeria Nuclear, Campus Nord B4-B5, Universitat Politècnica de Catalunya, E-08034 Barcelona, Spain*

(Dated: December 14, 2014)

We calculate the breathing mode frequency  $\omega$  in a one-dimensional Bose gas confined to a harmonic trap of frequency  $\omega_z$ . We predict a smooth crossover from Thomas–Fermi Bose–Einstein condensate (BEC) regime ( $\omega = \sqrt{3}\omega_z$ ) to Gaussian BEC regime ( $\omega = 2\omega_z$ ) using Hartree approximation and sum rules approach, adopted to small system sizes. Local density approximation (LDA) correctly captures the crossover from Tonks–Girardeau ( $\omega = 2\omega_z$ ) to Thomas–Fermi BEC ( $\omega = \sqrt{3}\omega_z$ ) regimes. Predictions from local density and Hartree approximations can be continuously matched for  $N \gtrsim 25$  particles, providing a complete zero-temperature description for large number of particles and resulting in a non-monotonic reentrant behavior of the breathing frequency. For smaller number of particles (ranging from  $N = 2$  to  $N = 25$ ) we perform extensive diffusion Monte Carlo simulations. This permits us to obtain a complete picture, applicable to arbitrary number of particles and any repulsive interaction strength. We provide perturbative analysis for both weak and strong coupling regimes. We revisit Innsbruck group experiment [Science **325**, 1224 (2009)], analyzing the measurements done in Thomas–Fermi — Gaussian BEC crossover, and demonstrate that the breathing frequency follows a reentrant behavior as a function of the interaction strength in full agreement with our theory.

PACS numbers: 71.10.Pm, 67.85.-d, 03.75.Hh,

Statistical properties of one-dimensional (1D) gases of quantum particles interacting through short-range potential are largely dependent on interaction strength. For a gas of bosons interacting through  $\delta$ -function potential of strength  $g > 0$  (repulsive Lieb–Liniger gas), increasing  $g$  suppresses spatial overlap between any two bosons [1]. This leads to a many-body excitation spectrum identical to that of a free Fermi gas, in the ultimate case of infinite repulsion,  $g = \infty$ , known as Tonks–Girardeau (TG) gas [2]. Hard-rods gas model, in which any boson cannot come within a distance smaller than the  $s$ -wave scattering length  $a_{1D}$  from any other boson, mimics ever stronger interparticle repulsion strength. And hard-rods gas model provides a good description for strongly attractive Lieb–Liniger gas prepared in some special highly excited state (super-TG gas) [3].

An interplay of interaction and statistical properties for quantum 1D gases is seen in a low-lying part of their excitation spectrum particularly well if the latter is discrete in the limit of large number of particles,  $N$ . The discreteness is ensured by confining quantum gas with the external potential. Ratio  $\omega/\omega_z$  of the frequency of the lowest compressional (breathing) mode,  $\omega$ , and the dipole mode,  $\omega_z$ , was investigated for a Lieb–Liniger gas confined by a parabolic potential in experiments [4–6]. It was observed that  $\omega/\omega_z$  goes through two crossovers: from 2 to  $\sqrt{3}$ , and then from  $\sqrt{3}$  to 2 as the system goes from non-interacting to weakly interacting, and then from weakly interacting to strongly interacting regime [5]. The latter crossover has been described theoretically, by the approach based on the local density

approximation (LDA) [7]. A description of the former crossover has not been done so far. Experiments [4, 6] have been done in the regime of weak coupling, for which  $\omega/\omega_z = \sqrt{3}$  is expected in the large  $N$  limit at zero temperature. To what extent are observed deviations from  $\sqrt{3}$  value due to finite  $N$  and temperature, is an open question answering which paves a way towards understanding equilibration and thermalisation benchmarks in dynamics of interacting quantum gases.

In this Letter we report analytic and numerical results for ratio  $\omega/\omega_z$  obtained within the repulsive Lieb–Liniger gas model for the parameters accessed in experiments [4–6]. We describe a crossover from non-interacting to weakly interacting gas analytically by making use of Hartree approximation for  $N \gg 1$ . Our Hartree solution connects smoothly with the one for weak to strong interaction crossover, obtained with LDA [7]. We complement analytic approaches with extensive diffusion Monte Carlo (DMC) simulations made for up to 25 particles, thus elaborating effects from finite  $N$ . Our zero-temperature results show perfect agreement with data from Innsbruck experiment [5]. On the other hand, we found a mismatch with those data points from Palaiseau group [6] which are away from mean-field prediction  $\omega/\omega_z = \sqrt{3}$ .

*Model.* — The model we consider is Lieb–Liniger gas of repulsive bosons in a parabolic trap. The Hamiltonian for  $N$  particles is

$$H = -\frac{\hbar^2}{2m} \sum_{i=1}^N \frac{\partial^2}{\partial z_i^2} + g \sum_{i<j} \delta(z_i - z_j) + \sum_{i=1}^N V(z_i). \quad (1)$$

Here  $m$  is the particle mass, and  $V(z) = m\omega_z^2 z^2/2$  is

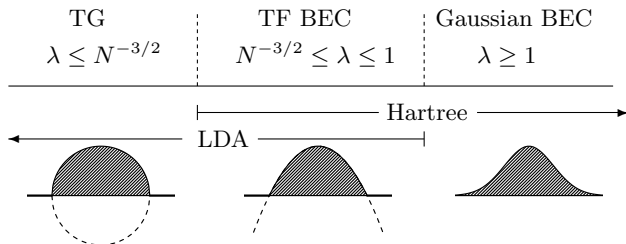


FIG. 1. Gaussian BEC, Thomas-Fermi BEC, and TG regimes of model (1) are shown as a function of Hartree parameter  $\lambda = -a_{1D}/(Na_z)$  for a given  $N$ . Density profiles are Gaussian, inverted parabola, and semicircle deep in these regimes, respectively.

the particle potential energy in a parabolic trap. Length scales in the model are set by the  $s$ -wave scattering length  $a_{1D}$ , related to the coupling constant  $g = -2\hbar^2/(ma_{1D})$ , and by the harmonic oscillator length  $a_z = \sqrt{\hbar/(m\omega_z)}$ .

Depending on  $a_{1D}$ ,  $a_z$ , and  $N$ , model (1) is in one of three zero temperature quantum regimes shown schematically in Fig 1: Gaussian Bose-Einstein condensate (BEC), Thomas-Fermi (TF) BEC, and Tonks-Girardeau (TG). Thermodynamic and local correlation properties of the model differ qualitatively between these regimes, see Ref. [8] and references therein.

First excited state of model (1), a dipole mode, is interaction-independent. It is associated with center-of-mass motion, which oscillates with the trap frequency  $\omega_z$ . Second excited state is doubly-degenerate for  $g = 0$  and  $g = \infty$ . One mode with interaction-independent frequency  $2\omega_z$  comes from center-of-mass motion. Another mode is the compressional mode, whose interaction-dependent frequency  $\omega$  is in the focus of the present Letter.

*Analytic approaches.* — Eigenfunctions and spectrum of model (1) are not known exactly for  $N > 2$ . To find  $\omega$  for arbitrary  $a_{1D}$ ,  $a_z$  and  $N$  we use sum rules approximation approach, reviewed in Ref. [9]. More specifically,  $\omega$  is obtained by calculating the response of the cloud size to a change of trap frequency  $\omega_z$ :

$$\omega^2 = -2 \frac{\langle Q \rangle}{\partial \langle Q \rangle / \partial \omega_z^2}, \quad (2)$$

where  $Q = Q_c \equiv \sum_{i=1}^N (z_i - Z_{cm})^2$ , and  $Z_{cm} = \sum_{i=1}^N z_i / N$  is the center of mass coordinate. The average  $\langle \dots \rangle$  is taken with respect to the ground state wave function  $\psi_{gs}(z_1, \dots, z_N)$  of Hamiltonian (1). Neglecting  $Z_{cm}$  in  $Q_c$  amounts to  $Q_c \rightarrow Q_0 \equiv \sum_{i=1}^N z_i^2$ , the latter operator being used in Ref. [7].

Varying  $\omega_z$  in Eq. (1) one generally excites many modes rather than a single breathing mode. Those modes led to a deviation of  $\omega$  given by Eq. (2) from its actual value, and their relative weight should thus be diminished by

a proper choice of  $Q$ . How good  $Q_c$  is for that purpose is seen by comparing the exact spectrum of our model for  $N = 2$  with  $\omega$  given by Eq. (2) for arbitrary ratio  $-a_{1D}/a_z$ . We found that  $\omega$  given by Eq. (2) with  $Q = Q_0$  misses up to 50% of the deviation from  $2\omega_z$  value, while with  $Q = Q_c$  it misses 4% at most.

To get  $\omega$  from Eq. (2) requires knowledge of ground state properties of Hamiltonian (1) only. Let us approximate  $\psi_{gs}$  (normalized to  $\langle \psi_{gs} | \psi_{gs} \rangle = 1$ ) with the Hartree variational wave function  $\psi_{gs}^H(z_1, \dots, z_N) = \prod_{i=1}^N \varphi(z_i)$ , which can be found explicitly by minimizing the functional  $E[\psi_{gs}^H] \equiv \langle \psi_{gs}^H | H | \psi_{gs}^H \rangle$  with respect to  $\varphi(z)$ . This procedure amounts to solving the Hartree eigenvalue equation

$$\left[ -\frac{1}{2} \frac{\partial^2}{\partial x^2} + \frac{x^2}{2} + \frac{2}{\lambda} |\varphi(x)|^2 \right] \varphi(x) = \epsilon \varphi(x) \quad (3)$$

for minimal possible energy  $\epsilon$ . Here the length  $x = z/a_z$ , and the energy  $\epsilon$  is measured in the units of  $\hbar\omega_z$ . The parameters  $a_{1D}$ ,  $a_z$ , and  $N$  enter Eq. (3) through a Hartree parameter

$$\lambda = -\frac{a_{1D}}{Na_z}. \quad (4)$$

We are assuming that  $N \gg 1$  when using Hartree approximation, and this assumption is incorporated into Eq. (3). Taking the average from Eq. (2) with respect to the Hartree state,  $\psi_{gs}^H$ , we get  $\langle Q_c \rangle = \langle Q_0 \rangle = \int dz z^2 n_H(z)$ , where  $n_H(z) = N |\varphi(z)|^2$  is the ground state density distribution within Hartree approximation. Therefore  $\omega/\omega_z$  is a function of single parameter  $\lambda$  within Hartree approximation.

Excitation spectrum of model (1) deep in Gaussian BEC regime,  $\lambda \gg 1$ , can be found perturbatively in  $g$ , resulting in

$$\omega^2 \simeq 4\omega_z^2 (1 - c_N \lambda^{-1}), \quad \lambda \rightarrow \infty, \quad (5)$$

where  $c_N = 1/\sqrt{8\pi}$  for all  $N \geq 2$ . Alternatively, the density profile from Eq. (3) can be used to evaluate the sum rules expression Eq. (2) to recover Eq. (5). Note, however, that Eq. (3) is written assuming that  $N \gg 1$  and thus gives  $c_N$  for  $N \rightarrow \infty$  only.

In the case of  $\lambda \ll 1$ , Eq. (3) results in an inverted parabola density profile (see Fig. 1)

$$n_H(z) = N \frac{(9\lambda)^{\frac{1}{3}}}{4a_z} \left( 1 - \frac{z^2}{Z^2} \right) \theta \left( 1 - \frac{z^2}{Z^2} \right), \quad \lambda \rightarrow 0. \quad (6)$$

Here the function  $\theta(x)$  is the Heaviside step function, and  $Z/a_z = (3/\lambda)^{1/3} \propto N^{1/3} \gg 1$ . Substituting Eq. (6) into (2) one gets  $\omega/\omega_z = \sqrt{3}$ , which is a characteristic of TF BEC regime. In case of arbitrary Hartree parameter  $\lambda$ , Eq. (3) is solved numerically, demonstrating a smooth monotonous increase of  $\omega/\omega_z$  with  $\lambda$ , until the value 2

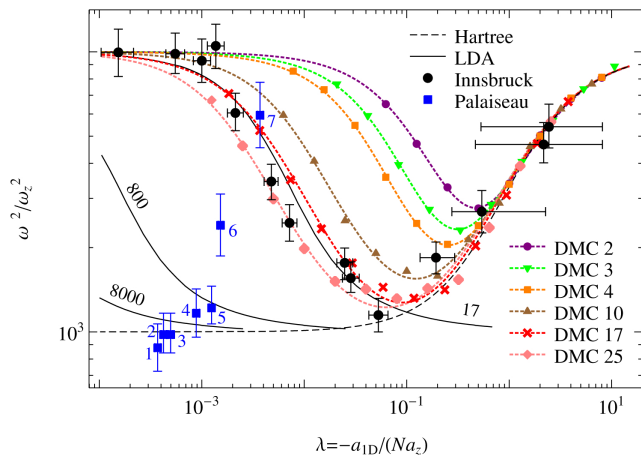


FIG. 2. (Color online) Ratio  $\omega^2/\omega_z^2$  as a function of Hartree parameter  $\lambda = -a_{1D}/(Na_z)$ . Black dashed line: Hartree approximation for  $N \rightarrow \infty$ . Black solid lines: LDA for  $N = 17, 800, 8000$ . Other dashed lines: interpolations for data points obtained with diffusion Monte Carlo (DMC) simulations for  $N = 2, 3, 4, 10, 17, 25$  particles (top to bottom). Large red circles: Innsbruck experiment [5]. Large blue boxes: Palaiseau experiment [6]. Gaussian BEC regime corresponds to  $\lambda \gtrsim 1$ , as defined from Fig. 1.

is reached deep in Gaussian BEC regime,  $\lambda \rightarrow \infty$ , see Fig. 2. Thus, Hartree approximation captures characteristic properties of TF BEC and Gaussian BEC regimes; the crossover takes place for the Hartree parameter  $\lambda \approx 1$  (see Figs. 1-2).

The crossover from TF BEC to TG regime for large  $N$  can be obtained within the local density approximation (LDA), which assumes that the local properties of the gas depend on its density,  $n = n(z)$ , at a given spatial point  $z$ . Local chemical potential  $\mu_{\text{loc}}$  is determined by the external potential,  $\mu_{\text{loc}}(n(z)) = V(Z) - V(z)$  for  $|z| \leq Z$ , in model (1). Here  $Z$  is the Thomas-Fermi radius of the gas cloud, whose value is set by normalization condition  $\int_{-Z}^Z dz n(\mu_{\text{loc}}(z)) = N$ . A dependence of  $\mu_{\text{loc}}$  on  $n$  follows from a solution of the homogeneous Lieb-Liniger model (Eq. (1) with  $V = 0$ ) given in Ref. [1]. Ratio  $\omega/\omega_z$  is calculated within LDA in Ref. [7], it depends on LDA parameter  $\Lambda = Na_{1D}^2/a_z^2$  [7, 10, 11].

Excitation spectrum of model (1) deep in TG regime,  $\Lambda \ll 1$ , can be found perturbatively in  $a_{1D}$ . For that we use a mapping from the gas of strongly repulsive bosons to that of weakly attractive fermions [12]. A perturbative solution for the ground state energy is given in Ref. [13]; analysis of excited states brings the result [14]

$$\omega^2/\omega_z^2 = 4 \left(1 - C_N \sqrt{\Lambda}\right), \quad \Lambda \rightarrow 0, \quad (7)$$

where  $C_N$  is calculated for all  $N \geq 2$ :

$$C_N = \frac{3\sqrt{2N}}{\pi\sqrt{\pi}} \frac{\Gamma(N - \frac{5}{2})\Gamma(N + \frac{1}{2})}{\Gamma(N)\Gamma(N + 2)} {}_3F_2 \left[ \begin{matrix} \frac{3}{2}, 1 - N, -N \\ \frac{7}{2} - N, \frac{1}{2} - N \end{matrix}; 1 \right]. \quad (8)$$

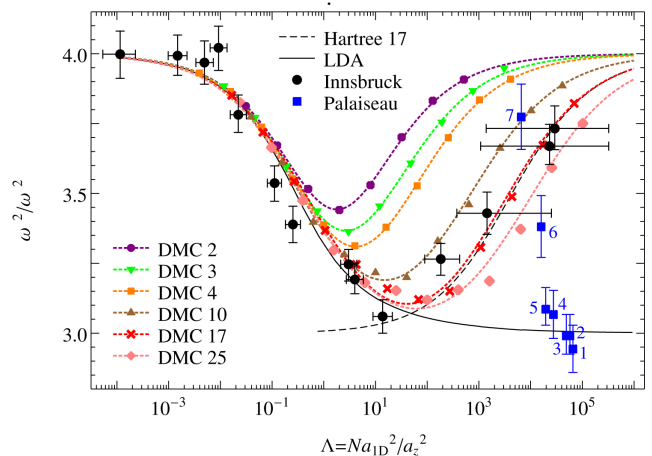


FIG. 3. (Color online) Ratio  $\omega^2/\omega_z^2$ , as a function of LDA parameter  $\Lambda = Na_{1D}^2/a_z^2$ . Black dashed line: Hartree approximation for  $N = 17$ . Black solid line: LDA for arbitrary  $N \gg 1$ . DMC and experimental data points are the same as shown in Fig. 2. TG regime corresponds to  $\Lambda \lesssim 1$ , as defined from Fig. 1.

Note that  $c_N$  entering Eq. (5) does not depend on  $N$ , while  $C_N$  does. The dependence is, however, very weak, and grows monotonously from  $C_2 = 1/\sqrt{4\pi} \approx 0.282$  to  $C_\infty = 32\sqrt{2}/(15\pi^2) \approx 0.306$ . The  $\Lambda \rightarrow 0$  expansion of the LDA solution reproduces Eq. (7) and the coefficient  $C_\infty$ . In the TG limit,  $\Lambda = 0$ , the local chemical potential is Fermi energy  $\mu_{\text{loc}} = (\pi\hbar n)^2/(2m)$ , resulting in semi-circular LDA density profile  $n(z) = \sqrt{2N - x^2}\theta(2N - x^2)/(\pi a_z)$ , with  $x = z/a_z$  (see Fig. 1).

In the case of  $\Lambda \gg 1$ , LDA implies Gross-Pitaevskii local chemical potential  $\mu_{\text{loc}} = gn$  and density profile defined by Eq. (6), characteristic of TF BEC regime. Solving Lieb's integral equations connecting  $\mu_{\text{loc}}$  and  $n$  numerically for arbitrary LDA parameter  $\Lambda$ , one gets  $\omega/\omega_z$  which goes down from 2 to  $\sqrt{3}$  as  $\Lambda$  goes from zero to infinity [7], as is seen in Fig. 3. Thus, LDA approximation indeed captures characteristic properties of TF BEC and TG regimes; a crossover value of LDA parameter  $\Lambda$  for these regimes is  $\Lambda \approx 1$  (see Figs. 1,3).

*DMC simulations.* — We complement the analytic results with large-scale numerical simulations based on diffusion Monte Carlo (DMC) algorithm [15]. That algorithm amounts to solving many-body Schrödinger equation in imaginary time and makes it possible to calculate ground state energy to arbitrarily high precision. The convergence rate of the simulations can be enhanced greatly by doing an importance sampling with a guiding wave function  $\psi_T$ . We use  $\psi_T(z_1, \dots, z_N) = \prod_{i=1}^N \exp(-c_{\text{var}} z_i^2) \prod_{j < k}^N (|z_j - z_k| - a_{1D})$ , with the parameter  $c_{\text{var}}$  minimizing the variational energy. This function is known to work very well in various 1D systems [16–19].

DMC algorithm is well suited for finding the ground-state properties while it is more challenging to find the

energies of the excited states and predict the breathing frequency. A possible way to do so is to use the inverse Laplace transform of imaginary-time correlation functions, as is done for  $N = 3$  atoms in Ref. [14]. However, the inverse Laplace transform is an exponentially ill-posed problem, as there are many real-frequency reconstructions which lead to essentially the same imaginary-time correlation function. This makes the inversion notoriously hard, especially for large number of particles where statistical noise increased. Instead, we rely on sum rules approach to relate the breathing frequency to static averages (2). This permits us to perform the calculations with system sizes  $2 \leq N \leq 25$ .

We plot the breathing frequency as a function of Hartree parameter  $\lambda$ , Eq. (4), in Fig. 2. One finds that in Gaussian BEC regime,  $\lambda \gtrsim 1$ ,  $\omega$  is indistinguishable from  $\omega^H$  for any  $N$ . Furthermore, the minimal value of  $\lambda$  at which  $\omega$  stays close to  $\omega^H$  decreases with increasing  $N$ , being about 0.1 for  $N = 25$ . The gas is deeply in the TF BEC regime at that point with  $\omega = \sqrt{3}\omega_z$ . The plot of  $\omega^H$  shown in Fig. 2 corresponds to the solution of Eq. (3) in the limit of  $N \rightarrow \infty$ .

*Comparison with experiments.* — Data points from Innsbruck [5] and Palaiseau [6] experiments are compared in Figs. 2 and 3 with our prediction from analytic and DMC approaches. Innsbruck group loaded BEC of  $^{133}\text{Cs}$  atoms into a two-dimensional array of optical traps. Each trap contained between 8 and 25 atoms, whose motion is confined to one spatial dimension. Very broad range of values of interatomic interaction strength was examined: from  $\gamma_0 = 5 \times 10^{-3}$  to  $\gamma_0 = 5 \times 10^2$ , where  $\gamma_0 = mg/(\hbar^2 n(0))$  is the dimensionless interaction strength in the trap centre. The increase of the argument of plots in Fig. 2,  $\lambda = -a_{1D}/Na_z$ , corresponds to decreasing  $\gamma_0$ , given that  $N$  is kept constant. The datapoints on the right part of that plot match well with  $\omega^2/\omega_z^2$  from Hartree approximation (black dashed line). Furthermore, DMC simulations for  $N = 17$  (red crosses) are in very good agreement with all experimental data. Letting  $N = 17$  in the LDA solution to the model (black solid line), we see that it agrees well with the experimental data points lying on the left part of Fig. 2. Finally, we find a good agreement between the experimental data and predictions of the Hartree approximation for  $N = 17$ , as can be seen in Fig. 3.

On the other hand Palaiseau group prepared single-tube system of the  $^{87}\text{Rb}$  gas using atom-chip setup. Interaction strength  $\gamma_0$  tuned with number of atoms  $N$ , given that  $a_{1D}$  is kept constant (see Table I). It is remarkable that all points but two last follows TF regime prediction.

When making comparison of our zero-temperature predictions with experiment, it is important to understand the role of the temperature. For the static properties, it is commonly considered that the quantum degenerate regime is reached when the temperature is be-

Point	1	2	3	4	5	6	7
$N \times 10^{-3}$	7.8	6.8	5.8	3.2	2.3	1.9	1.4
$\gamma_0 \times 10^3$	2.9	3.2	3.6	5.6	8.2	10	13

TABLE I. Data points from Palaiseau group [6], shown as large blue boxes in Figs. 2 and 3.

low the critical temperature of an ideal Bose gas  $T_Q = N\hbar\omega$ . In Palaiseau experiment [6] the temperature  $T = 100nK$  is well below the quantum degeneracy temperature,  $300nK < T_Q < 3000nK$ . From this point of view, the zero-temperature result  $\omega = \sqrt{3}\omega_z$  might be expected, instead points (6) and (7) significantly differ with the zero-temperature result. On the contrary, in Innsbruck experiment [5] the temperature  $T = 160nK$  is significantly higher than the temperature of the quantum degeneracy  $T_Q = 30nK$ . Nevertheless, the experimental points agree with our zero-temperature predictions within experimental error bars. It becomes clear, that the  $T_Q$  is not a proper parameter to compare with, when describing the dynamical properties.

Experimental data indicate dimensionless temperature  $t = 2\hbar^2 k_B T / (mg^2)$  to be in order of 1100 for Palaiseau and in range from  $3 \times 10^{-1}$  to  $3 \times 10^7$  for Innsbruck experiments. The particle number at crossover  $N_{co} = \frac{2}{3}t \ln(t/2) a_{1D}^2 / a_z^2$  [20] indicates crossover for  $^{87}\text{Rb}$  with 480 particles in the system. Thus system should be into the qBEC regime. Contrary for the data from Innsbruck in the weak coupling  $N_{co}$  is in range 30–130 thus due to [20] system should be in the decoherent regime.

*Summary.* — In this Letter we report frequency of the breathing mode for trapped 1D Bose gas. We revisit experiment [5] from Innsbruck group and demonstrate that the breathing frequency follows a reentrant behavior as a function of the interaction strength. We infer the breathing frequency from energy-level spacing (i) in perturbative calculations for strong repulsion and arbitrary number of atoms (ii) for arbitrary interaction and  $N = 2$  atoms. Alternatively, we use sum rules approach and demonstrate that by properly taking into account the center of mass contribution, very good accuracy is achieved (4% deviation at most for  $N = 2$  atoms). For large number of atoms, the breathing frequency decreases from  $\omega = 2\omega_z$  in Tonks-Girardeau regime (infinitely-strong repulsion) to  $\omega = \sqrt{3}\omega_z$  in Thomas-Fermi BEC regime. This crossover is correctly captured by local density approximation and is controlled by LDA parameter  $\Lambda = Na_{1D}^2/a_z^2$ . For even weaker interactions, the breathing frequency starts to increase until it reaches the maximal value of  $\omega = 2\omega_z$  in Gaussian BEC regime. This crossover is controlled by Hartree parameter  $\lambda = -a_{1D}/(Na_z)$ . Together, LDA and Hartree theories completely describe the breathing frequency for number of particles  $N \gtrsim 25$ . In order to complete the full descrip-

tion in terms of number of particles, we apply diffusion Monte Carlo method for  $2 \leq N \leq 25$  particles. We find that the breathing frequency follows a non-monotonic behavior, although TF BEC value,  $\omega = \sqrt{3}\omega_z$ , might be not reached. We revisit Innsbruck experiment [5] by analyzing the reported experimental points for which the increase in the breathing frequency was observed but no explanation was given. By presenting all experimental series on the same figure we find a good agreement between experimental data with our predictions in all regimes and thus demonstrate the reentrant behavior of the breathing mode.

We thank I. Bouchoule and B. Fang for useful discussions. Authors thank the Barcelona Supercomputing Center (The Spanish National Supercomputing Center – Centro Nacional de Supercomputación) for the provided computational facilities. The work of A. Gudyma was supported by grant from Region Ile-de-France DIM NANO-K. A.G.E. acknowledges partial financial support from the DGI (Spain) Grant No. FIS2011-25275 and Generalitat de Catalunya Grant No. 2009SGR-1003.

- 
- [1] E. H. Lieb and W. Liniger, *Phys. Rev.* **130**, 1605 (1963).
  - [2] M. Girardeau, *J. Math. Phys.* **1**, 516 (1960).
  - [3] G. E. Astrakharchik, J. Boronat, J. Casulleras, and S. Giorgini, *Phys. Rev. Lett.* **95**, 190407 (2005), [cond-mat/0405225](#).
  - [4] H. Moritz, T. Stöferle, M. Köhl, and T. Esslinger, *Phys. Rev. Lett.* **91**, 250402 (2003), [cond-mat/0307607](#).
  - [5] E. Haller, M. Gustavsson, M. J. Mark, J. G. Danzl, R. Hart, G. Pupillo, and H.-C. Nägerl, *Science* **325**, 1224 (2009), [1006.0739](#).
  - [6] B. Fang, G. Carleo, A. Johnson, and I. Bouchoule, *Phys. Rev. Lett.* **113**, 035301 (2014), [1312.3169](#).
  - [7] C. Menotti and S. Stringari, *Phys. Rev. A* **66**, 043610 (2002), [cond-mat/0201158](#).
  - [8] D. Petrov, D. Gangardt, and G. Shlyapnikov, *J. Phys. IV* **116**, 5 (2004), [cond-mat/0409230](#).
  - [9] J. W. Abraham and M. Bonitz, *Contrib. Plasma Phys.* **54**, 27 (2014).
  - [10] D. S. Petrov, G. V. Shlyapnikov, and J. T. M. Walraven, *Phys. Rev. Lett.* **85**, 3745 (2000), [cond-mat/0006339](#).
  - [11] V. Dunjko, V. Lorent, and M. Olshanii, *Phys. Rev. Lett.* **86**, 5413 (2001), [cond-mat/0103085](#).
  - [12] T. Cheon and T. Shigehara, *Phys. Rev. Lett.* **82**, 2536 (1999), [quant-ph/9806041](#).
  - [13] F. N. C. Paraan and V. E. Korepin, *Phys. Rev. A* **82**, 065603 (2010), [arXiv:1011.1706](#).
  - [14] Z. D. Zhang, G. E. Astrakharchik, D. C. Aveline, S. Choi, H. Perrin, T. H. Bergeman, and M. Olshanii, *Phys. Rev. A* **89**, 063616 (2014), [1312.7005](#).
  - [15] J. Boronat and J. Casulleras, *Phys. Rev. B* **49**, 8920 (1994), [cond-mat/9309015](#).
  - [16] G. E. Astrakharchik and S. Giorgini, *Phys. Rev. A* **68**, 031602 (2003), [cond-mat/0212512](#).
  - [17] G. E. Astrakharchik and S. Giorgini, *J. Phys. B: At. Mol. Opt. Phys.* **39**, S1 (2006), [cond-mat/0510463](#).
  - [18] G. E. Astrakharchik and I. Brouzos, *Phys. Rev. A* **88**, 021602 (2013), [1303.7007](#).
  - [19] M. A. Garcia-March, B. Julia-Diaz, G. E. Astrakharchik, T. Busch, J. Boronat, and A. Polls, *Phys. Rev. A* **88**, 063604 (2013), [1307.3510](#).
  - [20] I. Bouchoule, K. V. Kheruntsyan, and G. V. Shlyapnikov, *Phys. Rev. A* **75**, 031606 (2007), [physics/0611237](#).